the FEBS Journal

Chemical probing suggests redox-regulation of the carbonic anhydrase activity of mycobacterial Rv1284

Lisa Nienaber[1,*], Elysia Cave-Freeman[1,*], Megan Cross[1,*], Lyndel Mason[1], Ulla-Maja Bailey[1], Parisa Amani[1], Rohan A. Davis[1,2], Paul Taylor[3] and Andreas Hofmann[1,2,4]

1 Eskitis Institute, Griffith University, Nathan, Queensland, Australia
2 Queensland Tropical Health Alliance, Smithfield, Australia
3 School of Biological Sciences, The University of Edinburgh, Scotland, UK
4 Faculty of Veterinary and Agricultural Sciences, The University of Melbourne, Parkville, Victoria, Australia

Keywords
enzyme modulation; natural products; pH homeostasis; redox-regulation; β-carbonic anhydrase

Correspondence
A. Hofmann, Structural Chemistry Program, Eskitis Institute, Griffith University, N75 Don Young Road, Nathan, QLD 4111, Australia
Fax: +61 7 3735 6036
Tel.: +61 7 3735 4425
E-mail: a.hofmann@griffith.edu.au

*These authors contributed equally to this work

(Received 28 March 2015, revised 26 April 2015, accepted 28 April 2015)

doi:10.1111/febs.13313

The mycobacterial enzyme Rv1284 is a member of the β-carbonic anhydrase family that is considered essential for survival of the pathogen. The active site cavity of this dimeric protein is characterized by an exceptionally small volume and harbours a catalytic zinc ion coordinated by two cysteine and one histidine residue side chains. Using the natural products polycarpine and emodin as chemical probes in crystallographic experiments and stopped-flow enzyme assays, we report that the catalytic activity can be reversibly inhibited by oxidation. Oxidative conditions lead to the removal of one of the active site cysteine residues from the coordination sphere of the catalytic metal ion by engagement in a disulfide bond with another cysteine residue close by. The subsequent loss of the metal ion, which is supported by crystallographic analysis, may thus render the protein catalytically inactive. The oxidative inhibition of Rv1284 can be reversed by exposing the protein to reducing conditions. Because the physical size of the chemical probes used in the present study substantially exceeds the active site volume, we hypothesized that these compounds exert their effects from a surface-bound location and identified Tyr120 as a critical residue for oxidative inactivation. These findings link conditions of oxidative stress to pH homeostasis of the pathogen. Because oxidative stress and acidification are defence mechanisms employed by the innate immune system of the host, we suggest that Rv1284 may be a component of the mycobacterial survival strategy.

Database
Atomic coordinates and structure factors have been deposited in the Protein Data Bank under accession numbers 4yf4, 4yf5 and 4yf6.

Introduction

Carbonic anhydrases are metal-dependent enzymes catalyzing the reversible hydration of carbon dioxide to form the bicarbonate anion and a proton, thus being a pivotal enzyme class for carbon fixation and pH regulation in living organisms. Enzymes with carbonic anhydrase activity are separated into five different classes (α-ζ) [1,2]. With the exception of the ζ carbonic anhydrases, which use cadmium as an alternative metal co-factor [3], all other carbonic anhydrases are described as zinc-dependent. The seven human

Abbreviations
DSF, differential scanning fluorimetry; PDB, Protein Data Bank.

carbonic anhydrases belong to class α; β-carbonic anhydrases are found in algae, plants and bacteria [4], including mycobacteria. Rv1284 is included among the three genes in the *Mycobacterium tuberculosis* genome that code for proteins with similarities to carbonic anhydrases. The gene is required for optimal growth [5] and elevated levels of the gene product are found under starvation conditions, which are used to model persistent bacteria [6].

Despite the common features shared by α- and β-carbonic anhydrases, such as the catalytic activity of CO_2 hydration and the active site metal, there are also considerable structural differences. First, at the level of quaternary structure, β-carbonic anhydrases are oligomeric enzymes in solution; the fundamental structural unit is a dimer (Fig. 1a), although tetramers (Rv1284, Rv3588c) [7] and octamers (*Pisum sativum* β-carbonic anhydrase) [8] have also been observed. Second, there is a marked difference in the coordination of the active site metal. In mammalian carbonic anhydrases (α class), the protein provides coordinating ligands to the active site zinc ion by means of three histidine side chains. By contrast, β-carbonic anhydrases provide one histidine and two cysteine residue side chains as metal-coordinating groups (Cys35, His88, Cys91 in Rv1284) in the active state. Further coordination sites on the metal ion are occupied by at least one water molecule, consistent with the proposed zinc-hydroxide mechanism of CO_2 hydration. A blocked state of some β-carbonic anhydrases has been observed, whereby an aspartic acid residue (Asp37 in Rv1284) makes direct contact with the active site metal and thus completes the four-site coordination sphere without leaving access for water; a switch between both states has been proposed as a likely mechanism [8] and this is in agreement with experimentally obtained sigmoid enzyme activity curves [9] expected for mechanisms that switch between T- and R-states.

Oxidizing agents such as reactive oxygen and nitrogen species form part of the innate immune response by a host when invaded by a pathogen. This not only includes toxic molecules such as H_2O_2, NO and CO, but also molecular oxygen and acidic environmental pH. To survive this assault, pathogens have developed sensing and inactivation mechanisms that protect against this response by the host. In the case of *M. tuberculosis*, the environmental redox state is an important factor [10–14], besides nutrient starvation [6], for triggering the transition between its latent and active states. Despite the presence of mycobacterial enzymes that exert a protective function (such as superoxide dismutase, catalase, alkyl hydroperoxidase and peroxiredoxins), *M. tuberculosis* has been reported to lack the typical bacterial redox sensors (including *Salmonella* OxyR; *Rhizobium* FixL; *Escherichia coli* SoxR, fumarate/nitrate reduction regulator, ArcB; and *Streptomyces* RexA). Instead, the heme-conjugated histidine kinases DosS and DosT monitor the presence of oxidative ligands and regulate the DosR regulon [15,16].

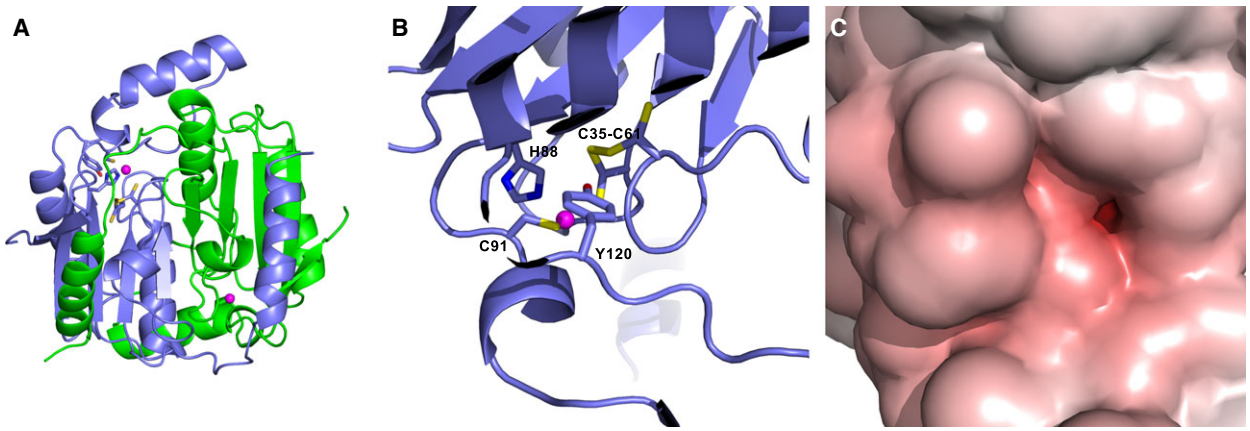

Fig. 1. Overview of structural features of Rv1284. (A) Rv1284 forms an intimate homodimer. The two monomers (dataset 4yf4) are shown as a cartoon representation and are coloured in blue and green, respectively. The active site residues, as well as Tyr120 of one monomer (blue), are drawn explicitly as stick models; the active site zinc ion is shown as magenta sphere. For the second monomer (green), the location of the active site is indicated by the rendered zinc ion. (B) A close-up of the active site of the blue monomer shows the relative orientation of Tyr120 with respect to the active site residues involved in zinc coordination. (C) This surface representation (the colour gradient indicates the electrostatic potential: blue, positive; red, negative) shows the same view of the monomer as in (B) and indicates the likely binding site of the chemical probes used in the present study. Images were rendered with PYMOL [41] and the electrostatic potential was calculated using PDB2PQR and APBS [42].

We recently proposed that β-carbonic anhydrases, in particular the mycobacterial enzymes Rv1284 and Rv3588c, may be targeted by nonclassical inhibitors that cause inhibition of the enzymatic function but do not bind in the active site of these enzymes [9]. During those efforts, we identified the previously reported cytotoxic marine natural product polycarpine, which possesses significant *in vivo* anti-tumour activity against P388 murine leukemia, and high inhibitory activity against reverse transcriptases from Raus sarcoma and avian myeloblastosis viruses *in vitro* and Na^+, K^+-ATPase isolated from rat brains [17–19]. The fact that polycarpine is a symmetrical disulfide, and therefore a potentially reactive molecule, led us to dismiss the compound as a lead compound for inhibitor design, and to use it instead as a probe molecule [20].

By chemical probing, we discovered that the mycobacterial carbonic anhydrase Rv1284 shows redox-dependent enzymatic activity and may thus be regulated by environmental redox conditions. One of the cysteine residues (Cys35) coordinating the catalytic zinc ion in the active site can be transformed into a cystine with residue Cys61 under oxidizing conditions. This leads to a loss of the catalytic metal ion and thus annihilation of the enzymatic activity of the protein. This oxidation may not only be initiated by air exposure (and thus also reactive species implicated in oxidative stress, such as H_2O_2), but also by peripheral ligands capable of undergoing redox reactions, such as the natural products polycarpine and emodin. The highly cytotoxic marine natural product polycarpine [17–19] is a symmetrically substituted disulfide; its oxidative effects are thus pH-dependent. Emodin is a polyhydroxylated anthraquinone that has been found in various plants such as *Rhamnus purshiana*, *Aloe* spp. and *Rumex* spp., as well as fungal sources such as *Penicillium* spp., *Aspergillus* spp. and *Dermocybe sanguinea* [21]. A variety of different biological activities has been reported for this secondary metabolite, including anti-microbial, anti-cancer and laxative effects [21]. Anthraquinones can easily be reduced to anthrahydroquinones and thus constitute oxidizing agents of significant strength.

Results

Detection of polycarpine interaction with His_6-Rv1284

To discover nonclassical inhibitors of β-carbonic anhydrases, we have established a programme in which an in-house compound library of pure natural compounds is screened against His_6-Rv1284 in thermal denaturation assays as a first step aiming to discover ligands interacting with the target protein [9,20]. Based on the results from these differential scanning fluorimetry (DSF) assays, polycarpine was identified as a ligand interacting with His_6-Rv1284 because it elicited a temperature shift of $\Delta T_m = -3.2$ K compared to the thermal denaturation of the protein in the absence of ligand.

Crystal structures of Rv1284 in the presence of polycarpine or H_2O_2

As reported previously [7], Rv1284 [Protein Data Bank (PDB) code: 1ylk] crystallizes in the orthorhombic space group F222 with two dimers in the asymmetric unit that are related by a crystallographic two-fold axis. Dimer formation is the result of intimate contacts between two monomers (Fig. 1a). This is achieved mainly by extending the five-stranded central β-sheet of one monomer to a 10-stranded β-sheet in the dimer. Furthermore, the N-terminal region of one monomer, which comprises 24 amino acids and includes an α-helix formed by residues Thr2-Phe18, is wrapped around the other monomer in a clamp-like fashion.

In an attempt to obtain ligand-bound crystal structures of mycobacterial carbonic anhydrase His_6-Rv1284 with ligands selected based on results from the DSF screening, polycarpine was subjected to co-crystallization experiments with the purified recombinant protein. Analysis of X-ray structures of crystals obtained under a variety of different conditions did not reveal electron density for a protein-bound ligand, and these were otherwise highly similar to the structure of the apo-protein. However, multiple conformations of residues in and around the active site of Rv1284 were observed (Fig. 2). In crystals obtained in the presence of polycarpine at the acidic pH 5.0 (PDB code: 4yf5), Cys35 was engaged in a disulfide bond with Cys61, a residue backing on to the active site. The occupancy of the cystine conformation at pH 5.0 was quantitative, depleting the active site metal centre of an essential coordinating group. The coordination site previously filled by the Cys35 thiolate was now occupied by a water molecule in some instances (molecules A and C in 4yf5) but led to departure of the zinc ion in others (molecules B and D in 4yf5). The absence of the active site metal, concomitantly, resulted in a widening of the active site cleft because the loop harbouring Cys91 shifted sidewards by approximately 1.5 Å (Fig. 3). However, overall, there were no significant structural changes observed compared to the apo-protein (PDB code: 1ylk), as indicated by the low rms

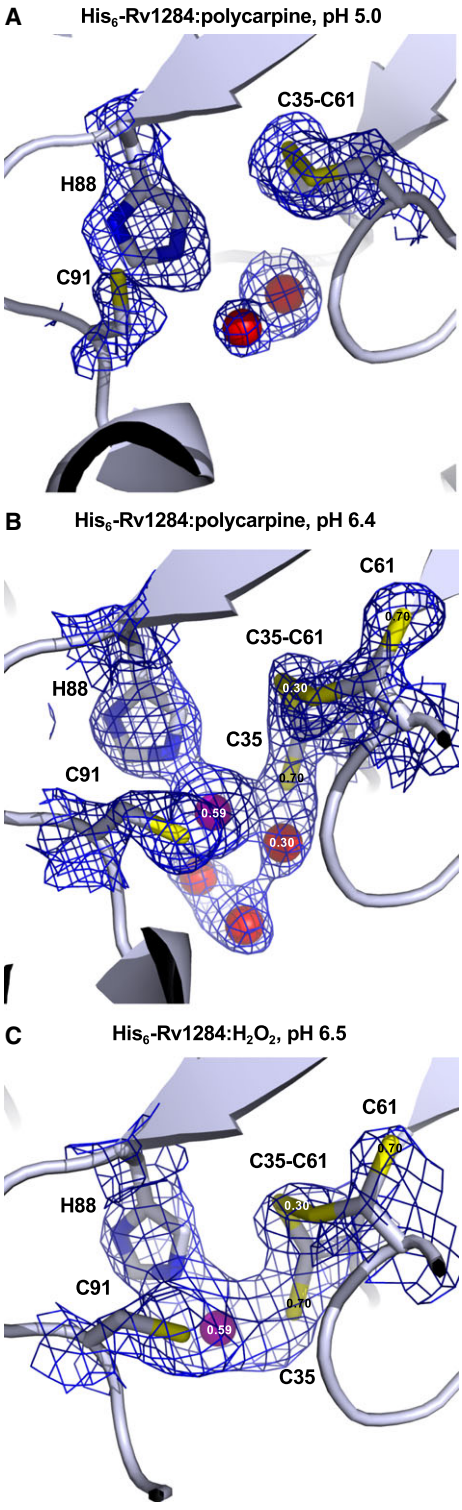

Fig. 2. The conformation in the active site of Rv1284 depends on the redox state. Stereo figures with $2F_o - F_c$ electron density (contoured at 1σ) show the active sites of three crystal structures: (A) His_6-Rv1284:polycarpine at pH 5.0 (PDB code: 4yf5); (B) His_6-Rv1284:polycarpine at pH 6.4 (PDB code: 4yf4); and (C) His_6-Rv1284:H_2O_2 at pH 6.5 (PDB code: 4yf6). The numbers indicate the occupancies of the individual atoms or conformations. Zinc is shown as magenta and water as red spheres. Images were rendered with PYMOL [41].

deviations (4yf5_A/1ylk_A: 0.21 Å; 1yf5_B/1ylk_B: 0.30 Å). At the mildly acidic pH 6.4 (PDB code: 4yf4), Cys35 existed in two conformations: one coordinating the active site zinc ion (60%) and another engaged in cystine formation with Cys61 (40%). Here, Cys61 took two conformations, one engaged in disulfide bond formation and one that was engaged in hydrogen-bonding to the backbone carbonyl of Leu86. When crystals of apo-His_6-Rv1284 obtained under very similar pH conditions were soaked for 10 min with 10 mM H_2O_2, the conformations observed in the active site of this crystal structure (PDB code: 4yf6) were essentially the same as for 4yf4, with two alternate conformations for Cys35 and Cys61.

Although crystals obtained from co-crystallization experiments were of good to very good quality, achieving diffraction resolutions of up to 1.8 Å, the peroxide-soaked crystals suffered from the treatment as reflected by the lesser resolution of 3.0 Å (Table 1). However, the electron density obtained after molecular replacement with the structure of the apo-protein clearly indicated the presence of a (partial) disulfide bond between Cys35 and Cys61.

Metal analysis of aged Rv1284 samples

Metal analysis of Rv1284 samples with a minimum shelf time of 2 weeks was carried out for zinc, iron and manganese using ICP-AES; 0.56 equivalents of zinc, 0.02 equivalents of iron and no manganese were found, confirming earlier reports of only partial occupancy of the Rv1284 active site by zinc [22]. The zinc content determined by ICP-AES is in excellent agreement with the occupancies determined for the active site zinc ions in the crystal structures, which range from 0.55 to 0.60.

Redox-dependency of Rv1284 enzymatic activity

The lack of significant enzymatic activity of N-terminally His-tagged Rv1284 in CO_2 hydration assays has been reported previously [7,9]. In the course of our drug discovery programme aiming to identify nonclassical β-carbonic anhydrase inhibitors, we observed that only freshly prepared untagged Rv1284 samples showed the expected catalytic activity in CO_2 hydration assays. Samples that were stored at 4 °C for

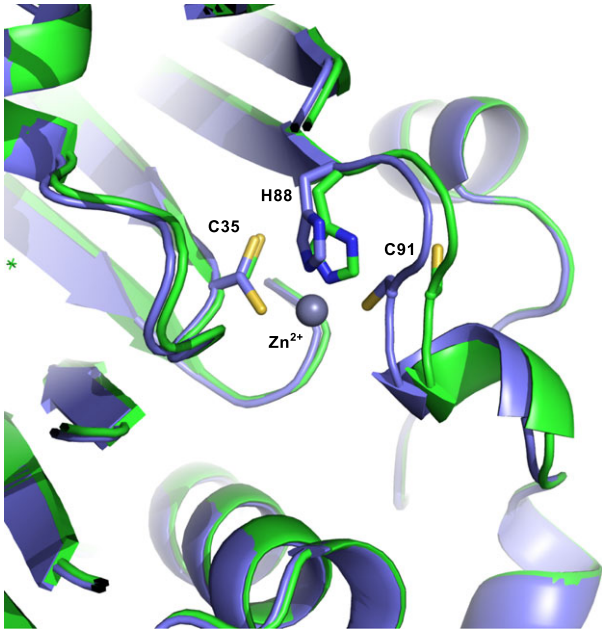

Fig. 3. Oxidation of Rv1284 can lead to loss of the catalytic zinc ion, which results in further conformational changes in the active site. Shown is a superposition of molecule B of the crystal structures obtained from His_6-Rv1284:polycarpine at pH 5.0 (PDB code: 4yf5; green) and His_6-Rv1284:polycarpine at pH 6.4 (PDB code: 4yf4; blue). Oxidation of Cys35 by polycarpine at acidic pH is quantitative and can result in the departure of zinc from the active site because of unsatisfying coordination. This leads to a widening of the active site cleft as the loop harbouring Cys91 shifts sidewards. Images were rendered with PYMOL [41].

longer than 2 weeks showed diminished or entirely abolished enzymatic activity. However, when purifying recombinant Rv1284 using N_2-saturated buffers, the shelf-life of active enzyme preparations was enhanced substantially, and a sample measured after a 10-week storage period at 4 °C still retained its original catalytic activity.

We then tested whether the enzymatic activity of aged Rv1284 samples could be recovered from inactive samples by exposing them to reducing conditions. An aliquot of an Rv1284 preparation (Fig. 4a, black filled circles) that lost activity because of storage for more than 2 weeks (Fig. 4a, black nonfilled circles) was incubated with DTT for 48 h, and a buffer-only sample of the same volume was subjected to the same protocol and used as a control. Because DTT interferes with the pH indicator monitoring in the CO_2 hydration assay, the reducing agent was removed by excessive washing of sample and control using ultrafiltration. The buffer-only control was tested in the assay to confirm the absence of any artificial effects. With the reductively re-activated sample of Rv1284, we observed enzyme activity at levels previously recorded for the freshly purified protein (Fig. 4a, green circles).

Incubation of an enzymatically active sample of Rv1284 with polycarpine in solution, in our hands, did not result in significant inhibition of enzymatic activity. The conditions tested included incubation times of up to 1 week and basic (pH 8.5) and mildly acidic (pH 6.5) buffers. We thus searched for organic molecules with known oxidative properties and a similar structural extent as that of polycarpine. Because the physical extent of such molecules exceeds the space provided in the very small active site cavity of mycobacterial carbonic anhydrases, these molecules cannot enter the active site of the folded protein. The anthraquinone emodin was chosen and, when incubating an enzymatically active preparation of Rv1284 (Fig. 4b, black circles) with 0.1 mM emodin at pH 8.5 for 1 week, the enzymatic activity was essentially abolished (Fig. 4b, blue circles). After subjecting the inactivated sample to DTT incubation (same procedure as above), the enzymatic activity of the sample was restored (Fig. 4b, green circles).

Based on these results, we decided to use emodin instead of polycarpine as a probe molecule in further enzyme activity assays. Because the crystallographic analysis identified Cys61 as the crucial residue in oxidative inactivation of Rv1284, the mutant Cys61Ser was generated to validate the role of this residue in the proposed mechanism. When tested in the CO_2 hydration assays, the mutant Rv1284-C61S showed activity that was indistinguishable from that of wild-type protein (Fig. 4c, black circles). Incubation of the mutant with emodin under the same conditions did not affect the enzymatic activity (Fig. 4c, blue circles).

A consequence of the hypothesis that molecules of the extent of emodin and polycarpine cannot migrate into the active site of mycobacterial carbonic anhydrases is the existence of a pathway by which two electrons can be withdrawn from the Cys35-Cys61 pair upon oxidation. Inspection of the crystal structure of Rv1284 suggested Tyr120 as a potential path (Fig. 1b,c). This residue shields the active site with its catalytic zinc ion from the protein surface and points its side-chain hydroxyl group into the active site, whereas its the backbone is surface-exposed. We therefore generated a Tyr120Leu mutant to assess the putative role of this residue. Figure 4d (black circles) shows the enzymatic activity of Rv1284-Y120L, which was very similar to that of the wild-type protein. After subjecting the mutant to emodin incubation under the same conditions as those described above, no change in the enzymatic activity was observed (Fig. 4d, blue circles), supporting the idea of Tyr120 being part of the electron pathway.

Table 1. X-ray crystal structure data collection and refinement statistics.

Dataset	4yf5 His_6-Rv1284:polycarpine (pH 5.0)	4yf4 His_6-Rv1284:polycarpine (pH 6.4)	4yf6 His_6-Rv1284:H_2O_2 (pH 6.5)
Crystallization conditions	15% poly(ethylene glycol) 400, 0.1 M NaH_2PO_4/Na citrate, pH 5, 10 mM polycarpine	0.10 M K/Na tartrate, 0.10 M Mes/NaOH, pH 6.4, 10 mM polycarpine	0.2 M NaF, 20% poly(ethylene glycol) 3500, 0.1 M Bis-Tris propane, pH 6.5; soaked with 10 mM H_2O_2 for 10 min
Data collection			
X-ray source	AS MX1	AS MX1	AS MX1
Detector	ADSC Quantum 210r	ADSC Quantum 210r	ADSC Quantum 210r
Wavelength (Å)	0.95375	0.95382	0.95375
Space group	F222	F222	F222
Cell dimensions (Å)	103.3, 153.9, 159.1	101.1, 154.4, 157.7	101.1, 153.9, 157.2
Maximum resolution (Å)	2.0	1.8	3.0
$<<I>/<\sigma(I)>>$	22.6 (5.1)	15.0 (1.8)	14.2 (4.9)
Wilson B-factor ($Å^2$)	27.6	22.2	47.9
Number of unique reflections	42 879 (5941)	56 222 (7594)	12 412 (1777)
Multiplicity	13.7 (12.7)	5.4 (3.1)	14.9 (14.6)
Completeness	0.992 (0.949)	0.988 (0.924)	0.997 (0.994)
R_{sym}[a]	0.074 (0.459)	0.06 (0.448)	0.207 (0.581)
Refinement			
Number of reflections in working/test set	39 382/2062	49 462/2669	11 220/577
Number of nonhydrogen protein atoms	5084	5108	5108
Visible residues	1–163	1–163	1–163
Number of water molecules	249	321	1
Number of ions	4 (2 × Zn^{2+}, 2 × Cl^-)	10 (4 × Zn^{2+}, 4 × Mg^{2+}, 2 × Cl^-)	8 (4 × Zn^{2+}, 2 × Mg^{2+}, 2 × Cl^-)
Average B-factor ($Å^2$)			
Protein	29.8	24.4	22.5
Solvent	28.6	28.0	32.4
Ions	31.4	27.5	37.0
rmsd B-factor for bonded atoms ($Å^2$)	4.96	4.30	8.40
rmsd bond lengths (Å)	0.008	0.008	0.009
rmsd bond angles (°)	1.113	1.096	1.172
MOLPROBITY analysis			
Ramachandran favoured (%)	96.7	99.7	94.0
Ramachandran allowed (%)	3.26	0.31	5.40
Ramachandran outliers (%)	0	0	0.6
Rotamer outliers (%)	3.55	4.6	7.7
C-beta outliers	0	0	0
Clashscore	5.13	3.33	8.14
Overall score	1.93	1.58	2.52
R_{factor}[b]	0.197 (0.268)	0.194 (0.305)	0.167 (0.268)
R_{free}[c]	0.260 (0.313)	0.244 (0.324)	0.260 (0.356)

Values in parentheses refer to the last resolution shell. [a] $R_{sym} = \Sigma|I - <I>|/\Sigma I$, where I is the observed intensity and $<I>$ is the average intensity obtained from multiple observations of symmetry-related reflections after rejections. [b] $R_{factor} = \Sigma||F_o| - |F_c||/\Sigma|F_o|$, where F_o and F_c are the observed and calculated structure factors, respectively. [c] R_{free} defined in Brünger [40].

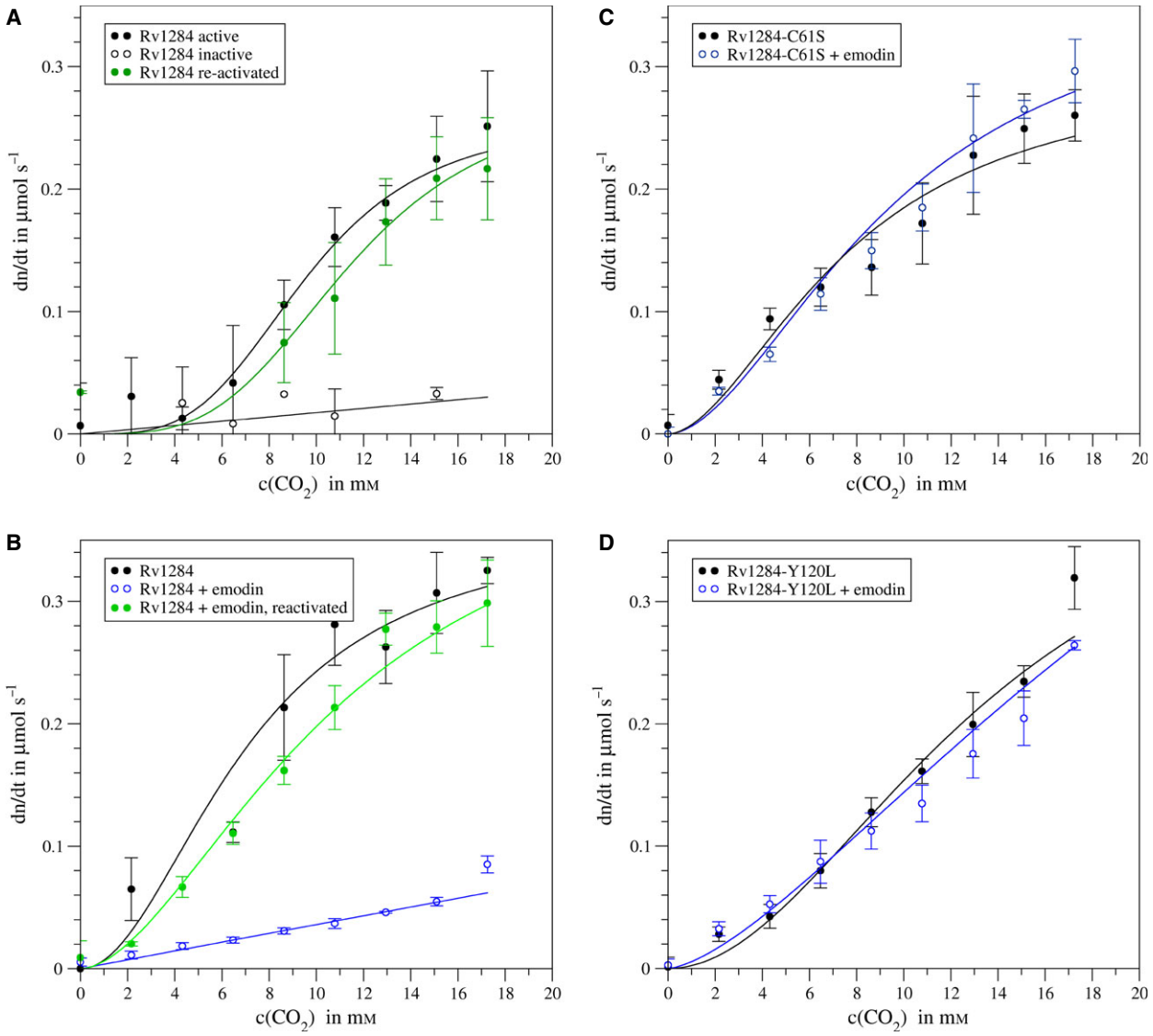

Fig. 4. Stopped-flow measurements assessing the catalytic CO_2 hydration activity by Rv1284 proteins. (A) Oxidation of Rv1284 during storage results in loss of the CO_2 hydration activity, which can be restored by the addition of reducing agents. Michaelis–Menten profiles of the enzymatic CO_2 hydration activity of purified recombinant Rv1284 were acquired using freshly purified protein (black filled circles, 'active'), the same sample after 2 weeks of storage (black nonfilled circles, 'inactive') and inactive protein after treatment with DTT (green filled circles, 're-activated'). (B) Oxidation of Rv1284 with 0.1 mM emodin at pH 8.5 for 1 week results in loss of the CO_2 hydration activity, which can be restored by the addition of reducing agents. Michaelis–Menten profiles of the enzymatic CO_2 hydration activity of freshly purified recombinant Rv1284 (black filled circles) and after incubation with emodin (blue nonfilled circles). Incubation of the emodin-treated sample [same conditions as in (A)] with DTT restores enzymatic activity (green filled circles). (C) Cys61 is critical for the redox-dependent regulation of Rv1284 enzymatic activity. The mutant Rv1284-C61S displays CO_2 hydration activity similar to the wild-type protein (black filled circles). Incubation of Rv1284-C61S with emodin [same conditions as in (A)] does not affect the enzymatic activity of the protein (blue nonfilled circles). (D) The electron transfer pathway involves Tyr120. The mutant Rv1284-Y120L displays CO_2 hydration activity similar to the wild-type protein (black filled circles). No significant effect on the enzymatic activity of the mutant is observed after incubation of Rv1284-Y120L with emodin [blue nonfilled circles; same conditions as in (A)].

Discussion

Our ongoing efforts to discover nonclassical inhibitors of mycobacterial carbonic anhydrases are based on screening natural product-derived compound libraries by DSF as a first-line experiment to identify potential effectors for the β-carbonic anhydrases Rv1284 and Rv3588c. The cytotoxic marine natural product polycarpine was identified in these thermal stability assays

using His_6-Rv1284, and thus subjected to co-crystallization experiments using His_6-Rv1284 and His_6-Rv3588c. Protein crystallography support of drug discovery for mycobacterial carbonic anhydrases has proved to be difficult because, to our knowledge, organic molecules containing more than six atoms have not been observed in ligand-bound protein crystal structures so far.

The crystal structures of purified bacterially expressed His_6-Rv1284 under ambient conditions (i.e. without the addition of oxidizing or reducing agents) showed an active site conformation where a partially occupied catalytic metal site is coordinated by the three conserved active site residues of β-carbonic anhydrases (Cys35, His88 and Cys91 in Rv1284). The presence of Cys61 in the loop region between strand β2 and helix α3 allows for an oxidized conformation of Cys35 by means of disulfide bond formation because Cys61 backs on to the active site and both cysteine side chains can adopt cystine conformation by a simple rotation around the Cα-Cβ bond. This oxidized state of the active site could be achieved by a redox reaction with small molecules that can enter the constrained active site, such as H_2O_2 (PDB code: 4yf6). Intriguingly, the same effect could be elicited by redox-active substrates that are highly unlikely to enter the active site, as observed in the present study serendipitously with polycarpine (PDB code: 4yf4). Because of the size and extent of polycarpine, there is no obvious access route for this molecule to the active site of Rv1284 without major conformational changes.

Since no substantial rearrangements of the protein fold were observed in the crystal structure obtained in the presence of polycarpine (PDB code: 4yf4), we conclude that the reduction of polycarpine occurs as a half-reaction at the protein surface and its redox potential should thus be pH-dependent because protons delivered by the bulk solvent will be consumed (Fig. 5). This expected pH-dependence is in agreement with the crystal structure obtained in the presence of polycarpine at low pH (PDB code: 4yf5), where the quantitative cystine formation was observed, that even led to loss of the catalytic metal ion.

These crystallographic results suggest that Rv1284 is an enzyme that is subject to oxidative inactivation. Indeed, when conducting CO_2 hydration assays with purified bacterially expressed Rv1284, we found that samples with a shelf life of more than 2 weeks lost enzymatic activity (Fig. 4a), which may be explained by oxidation as a result of air contact. The idea of oxygen-induced inactivation is further supported by the prolonged shelf-life of samples that had been subjected to protection with nitrogen gas during purification. The enzymatic activity of inactivated protein samples could be restored by exposing those samples to reducing conditions (Fig. 4a) and the crucial role of Cys61, which we consider to render a dysfunctional active site upon disulfide bond formation with Cys35, is evident from the crystal structures (Fig. 2), as well as enzyme assays using a Cys61Ser mutant (Fig. 4c).

The incubation of Rv1284 with polycarpine in solution for up to 1 week did not substantially affect the enzymatic activity of the protein neither under acidic nor basic conditions. This was a rather unexpected observation because the compound had an oxidizing effect in the crystal structures (Fig. 2). However, the polycarpine-modified crystals of Rv1284 were only obtained after approximately 3 months from co-crystallization experiments. The exposure time of protein and compound in the crystallization experiments is thus substantially longer than in the experiments testing enzyme activity. We therefore aimed to replace polycarpine with another probe compound that possesses strong oxidative properties and a sufficient size meaning that it is not able to migrate into the active site of Rv1284. Both criteria led us to choose emodin, which, as expected, affects Rv1284 enzymatic activity by means of reversible oxidative inactivation (Fig. 4b).

If ligands such as polycarpine and emodin indeed modify the conformation in the active site from a surface location on the protein, there must be a path by which electrons are channelled into/out of the active site cysteine Cys35. Inspection of the crystal structure highlighted Tyr120 as a possible electron-conducting residue (Fig. 1b,c). To test this hypothesis, we constructed the mutant Tyr120Leu, which was expected to restrict electron channelling in this location and thus render the protein largely in-susceptible to oxidative inactivation by surface-bound effectors. Figure 4d illustrates the results from enzyme activity assays with the mutant Tyr120Leu and validates the crucial role of tyrosine 120 in this context.

Although the amino acid sequence alignment of β-carbonic anhydrases suggested that other members of this enzyme family may potentially possess a similar redox feature to that of Rv1284, a rigorous structure-based analysis showed that this is not the case (Fig. 6). At present, there are three enzymes with known three-dimensional structures that possess a cysteine residue in the loop region between β2 and α3: *Porphyridium purpureum* (1ddz; Cys177, Cys203), *Saccharomyces cerevisae* Nce103 (3eyx; Cys84) and *Sordaria macrospora* (4o1k; Cys85). However, none of these residues are located spatially close enough to

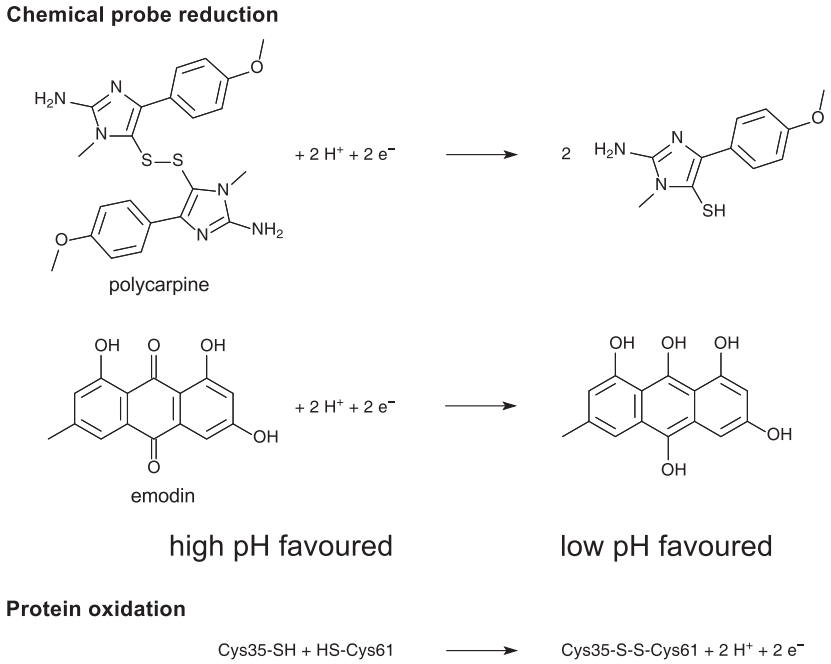

Fig. 5. Structures of the chemical probes polycarpine and emodin, and their redox reaction with mycobacterial Rv1284. Polycarpine is a symmetrical disulfide that can be reduced by withdrawing electrons from Rv1284, whereby Cys35 and Cys61 undergo an oxidation to form a cystine. The reduction of polycarpine is pH-dependent and the reduced form is favoured at lower pH. Therefore, formation of the Cys35-Cys61 cystine is enhanced at acidic pH, in agreement with the observation made in crystal structures obtained at pH 6.4 (PDB code: 4yf4) and pH 5.0 (PDB code: 4yf5). The anthraquinone emodin is a powerful oxidation agent because it can readily be reduced to an anthrahydroquinone. In the present study, emodin was used to oxidize Rv1284 in solution.

engage in a cystine formation with the active site cysteine residue (Fig. 6). Among the currently known β-carbonic anhydrases, Rv1284 from *M. tuberculosis* thus appears to be the only enzyme that engages this particular redox-regulation of enzymatic activity.

Conclusions

The discovery that the enzymatic activity of Rv1284 is susceptible to redox conditions invites speculations regarding the physiological significance of this mechanism, linking oxidative stimuli to changes in the pH homeostasis of the pathogen. Oxidative stress and acidification are central components of the innate immune system by which the host responds to pathogens [23]. There is thus a widely held view that acid and other host defences, such as reactive oxygen species and reactive nitrogen intermediates, act in synergy. Because oxidative inactivation of Rv1284 interrupts the enzymatic hydration of CO_2 and thus the production of protons, the lowering of the pH within the radius of action of Rv1284 would be halted. The redox-regulation of Rv1284 may thus be a component of the mycobacterial survival strategy. Intriguingly, the molecular workings of this mechanism resembles what has been observed with the zinc-associated anti-σ factor RslA. Mycobacterial RslA and the transcription factor σ^L are part of the transcription machinery that responds to oxidative stimuli. In RslA, residues from the CXXC motif can form a vicinal disulfide bond leading to dismissal of the bound zinc ion, which in turn disengages RslA from σ^L as a result of conformational changes on RslA [24].

Furthermore, in the absence of any ligand-bound crystal structures of mycobacterial carbonic anhydrases with small-molecule compounds possessing more than six atoms, the present study provides a first mapping of a ligand binding site on the surface of Rv1284, namely in an area around Tyr120.

Materials and methods

Cloning and mutagenesis of expression constructs

The cDNA construct of N-terminally His_6-tagged Rv1284 in pCR-T7 [22] was a kind gift from T. A. Jones (University of Uppsala, Sweden). This construct was used for sub-

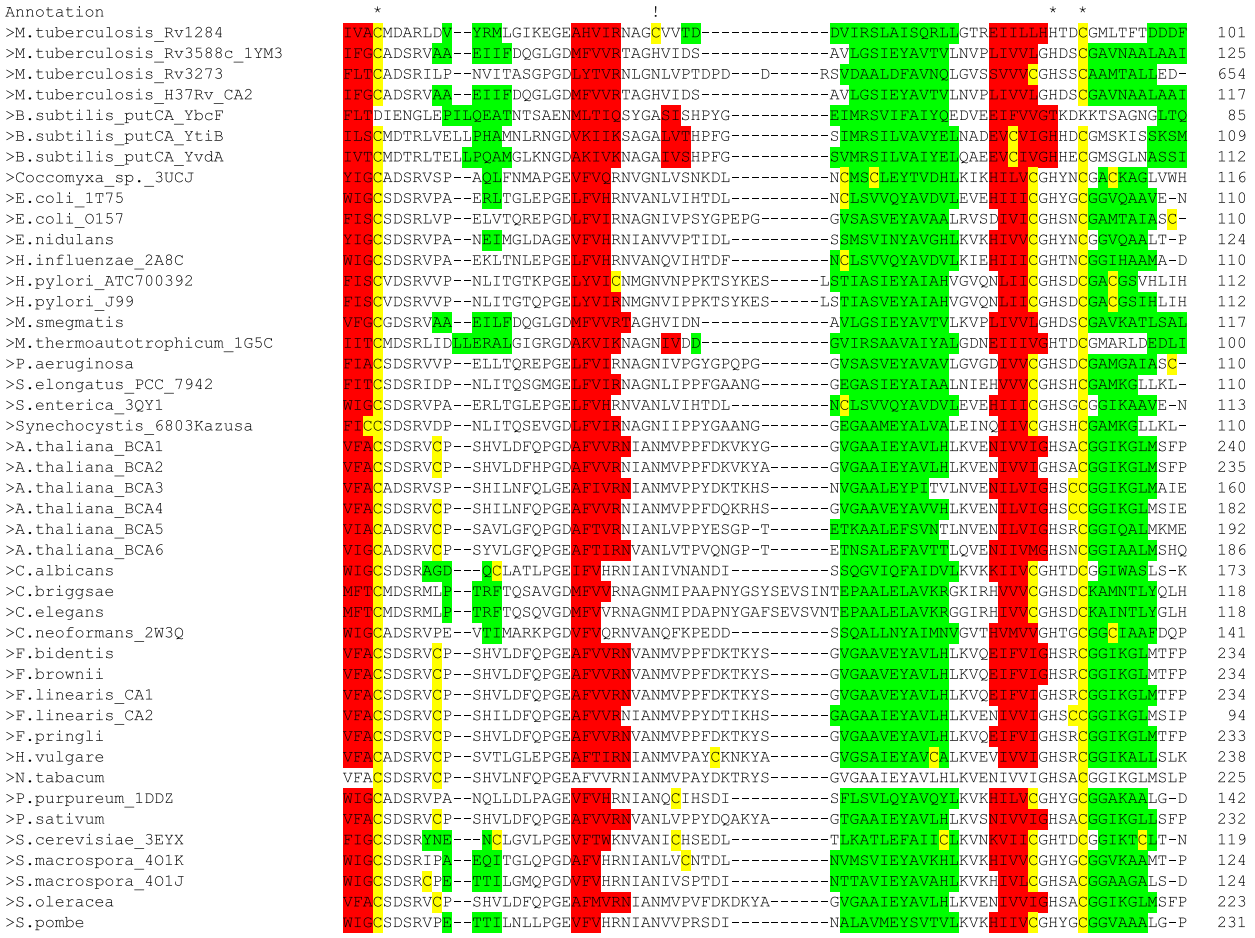

Fig. 6. Excerpt from a structure-based amino acid sequence alignment of β-carbonic anhydrases generated with SBAL from PDB files [37,39] or PSIPRED [38] secondary structure predictions using amino acid sequences. The amino acid sequence alignment from the superimposed three-dimensional structures of β-carbonic anhydrases shows that the cysteine residue in the active site is too distant from the cysteine residue in the loop region between β2 and α3 to engage in cystine formation. Only in the case of Rv1284 is Cys61 spatially close enough to form a covalent bond.

cloning of untagged Rv1284 into pRSET_6c [25] as described previously [9]. Mutant constructs of Rv1284 were generated by the QuickChange® (Stratagene, La Jolla, CA, USA) method, which is based on inverse PCR [26]. A pair of homologous primers (C61S mutation, coding: 5′-C AAC GCC GGA TCC GTG GTC ACC GAC GAT GTG ATC CGT TCA CTG-3′; C61S mutation, noncoding: 5′-GTC GGT GAC CAC GGA TCC GGC GTT GCG GAT GAC GTG TG-3′; Y120L mutation, coding: 5′-GG TCG CCC GA*A AGC TTG* CCC GAC GCC GTC GAG GAC GTC CG-3′; Y120L mutation, noncoding: 5′-C GGC GTC GGG C*AA GCT T*TC GGG CGA CCA CGT GGG TCT G-3′) carrying the mutations were designed for each mutant protein, and used in a PCR reaction performed with PfuUltra II Fusion HS DNA Polymerase (Agilent Technologies, Integrated Sciences Pty Ltd, Preston, VIC, Australia). The PCR product was then treated with *Dpn*I to digest the parental DNA template prior to transformation into chemically competent *E. coli* XL1Blue cells generated in house. Single colonies were picked, propagated and cDNA was purified using the NucleoBond Xtra kit (MN; Scientifix Life, Brisbane, QLD, Australia). All constructs were validated by DNA sequencing using BigDye chemistry (Applied Biosystems, Foster City, CA, USA).

Preparation of recombinant proteins

Bacterially expressed recombinant N-terminally His_6-tagged Rv1284 and untagged Rv1284 were produced and purified as described previously [9]. Briefly, the expression plasmids were transformed into *E. coli* BL21-AI, and a total of 8 L of LB+ medium [27] and 50 $\mu g \cdot mL^{-1}$ ampicillin were inoculated with 1 : 10 of its volume from an overnight liquid culture. Cells were grown at 37 °C for 4 h and then

induced with either 0.2% arabinose (His_6-Rv1284) or 0.2% arabinose and 0.5 mM IPTG (untagged Rv1284). After another 4 h of incubation at 37 °C, cells were harvested, resuspended in 100 mM NaCl, 1 mM EDTA, 20 mM Tris (pH 8), 0.1% Triton X-100, 1 mM PMSF, 5 mM benzamidinium chloride and subsequently lyzed by multiple freeze–thaw cycles and sonication. The cell lysate was subjected to ultracentrifugation (100 000 ***g*** for 45 min at 4 °C) and proteins purified by either Ni^{2+} affinity chromatography (His_6-Rv1284) or ion exchange chromatography (untagged Rv1284). The purified protein samples were concentrated by ultrafiltration. In the final cycles, the buffer was exchanged to 2% glycerol, 100 mM NaCl, 20 mM Hepes (pH 7.5). All purification steps were monitored by SDS/PAGE.

For N_2-saturated buffers, MilliQ water (Millipore, Billerica, MA, USA) was first degassed and then saturated with N_2 by injecting a stream of N_2 gas for 30 min. Working buffers were constituted from highly concentrated stock solutions of ingredients, diluted with N_2-saturated water.

Metal analysis

Metal content analysis of bacterially expressed and purified Rv1284 ($\rho^* = 1$ mg·mL^{-1}) was carried out using inductively coupled plasma atomic emission spectroscopy for zinc, manganese and iron with an Optima 8300 instrument (Perkin Elmer, Glen Waverley, VIC, Australia). Calibration curves were obtained using serial dilutions of 1000 p.p.m. standards (ICP-OES analytical standards; Perkin Elmer) for these metals.

Chemicals

The in-house natural product library used in this study consists of some 350 distinct and purified compounds, most of which have been obtained from Australian natural sources, and a small percentage (approximately 5%) are known commercial drugs or synthetic compounds inspired by natural products. The library included the *bis*-TFA salt of polycarpine, which was isolated from several *Polycarpa* spp. collected on the Great Barrier Reef, as well as emodin (#E7881), which was sourced from Sigma-Aldrich (Castle Hill, NSW, Australia).

DSF

The optimal ratio of protein and fluorescence dye was optimized by testing a 4 × 5 matrix of conditions varying the protein concentration from 2.5 to 40 μM, and SYPRO Orange (Invitrogen; Life Technologies, Mulgrave, VIC, Australia) concentration between ×5 and ×20, using a sample volume of 20 μL with a buffer composed of 100 mM NaCl and 20 mM Hepes (pH 7.5). For Rv1284, the best conditions were determined to contain 40 μM protein and 6.5× SYPRO Orange. At least three technical replicas were then tested for for each ligand using the optimized protein : dye ratio. Ligands were added at a final concentration of 250 μM in 20-μL sample aliquots, with a final DMSO concentration of 5%. Experiments were conducted on a Roche LightCycler 480, (Roche, Basel, Switzerland) and analyzed using DMAN [28]. ΔT_m values were calculated as difference between ligand and DMSO control experiments.

Protein crystallography

Crystals of N-terminally His_6-tagged Rv1284 were obtained from a variety of different conditions, all of which belonged to the orthorhombic space group F222. The crystallization conditions of the different datasets are provided in Table 1. All crystals used in the present study were obtained by the sitting drop vapour diffusion method with crystallization experiments carried out at 16 °C.

X-ray diffraction data were collected using the in-house diffractometer (MicroMax007-HF; R-Axis IV++ detector; X-stream cryo equipment; Rigaku Corp., Tokyo, Japan) and at the Australian Synchrotron beamline MX1 [29] under cryogenic conditions ($T = 100$ K). Datasets were indexed with XDS [30], and scaling, truncation and analysis were performed using the CCP4 suite [31]. The orthorhombic crystal structures with four molecules per asymmetric unit were solved by molecular replacement using an Rv1284 dimer model of PDB code: 1ylk [22]. Model building was performed with O [32] and COOT [33] and interspersed with computational refinement of atomic positions, individual B-factors and TLS refinement with two groups (chains A, B and chains C, D) using PHENIX [34]. The occupancies of active site metal ions, as well as residues with multiple conformations, were also subjected to refinement. We note that, in dataset 4yf4, a residual positive $F_o - F_c$ density remains in close spatial vicinity of Cys35-Sγ, a site that is partially occupied by a water molecule when Cys35 is engaged in disulfide bond formation with Cys61. We assume that this water molecule coordinates the zinc ion in the active site in the absence of Cys35-Sγ and the metal ion is present in the active site. Neither averaged maps (calculated with PHENIX), composite omit maps (calculated with CNS) [35], nor modelling of the partially occupied water molecule with Cl^- resulted in a reasonable and more sophisticated model. The geometry of the final models was scrutinized using MOLPROBITY as implemented in PHENIX [34].

Enzyme activity assays

To analyze the CO_2 hydration kinetics catalyzed by Rv1284, a stopped flow assay with pH indicator readout

was employed [36]. The absorbance change of *m*-cresol purple at a wavelength of 572 nm was monitored using a SFM-100 MOS LED stopped flow instrument (Bio-Logic SAS, Claix, France). CO_2 was obtained from BOC (North Ryde, NSW, Australia), and all solutions were made with freshly filtered and degassed deionized water. A stock solution of polycarpine was prepared in DMSO at a concentration of 60 mM; the stock of 60 mM H_2O_2 was prepared freshly as aqueous solution. For an individual experiment, the sample buffer contained 100 mM Na_2SO_4, 25 mM Taps (pH 8.5), 50 μM *m*-cresol purple, 5 μM protein and various additions as specified. The substrate buffer consisted of CO_2-saturated water to achieve final concentrations of between 2 and 17 mM. The reactions were followed for the first 60 s, and at least five traces were analyzed for each individual experiment to determine the initial rates of the reaction.

Reduction of protein samples

Aliquots (500 μL at 18–24 mg·mL^{-1}) of Rv1284 wild-type and mutant protein samples that had been subjected to enzyme activity assays were incubated with 0.1 mM DTT for 48 h. A buffer sample of the same volume was also incubated with DTT at the same concentration and used as a control. DTT was then removed from all samples by successively washing (10×) with degassed buffer in an ultrafiltration device.

Bioinformatic methods

A total of 40 curated β-carbonic anhydrase sequences were extracted from UniProtKB based on an annotation search, and combined with additional sequences obtained from the PDB. Nonredundant secondary structure-based amino acid sequence alignments were generated using SBAL [37] and secondary structure information either predicted with PSIPRED [38] or extracted from PDB files [39].

Acknowledgements

We gratefully acknowledge James Cameron (Griffith University) for help with the ICP-AES measurements, as well as Graeme Stevenson (Eskitis Institute) for useful discussions. Research in the laboratory of AH is funded by the National Health and Medical Research Council (NHMRC), the Australian Research Council (ARC) and the Rebecca L. Cooper Medical Research Foundation. RAD wishes to acknowledge the NHMRC (APP1024314) and ARC (LP120200339) for funding. Parts of this research were undertaken on the MX1 beamline at the Australian Synchrotron (Clayton, VIC, Australia).

Author contributions

LN and ECF performed the enzyme assays. MC, LM and UMB cloned and expressed the proteins. MC and AH collected diffraction data and AH solved the crystal structures. RAD provided the natural products. PA, RAD, PT and AH analyzed the data. AH conceived the study and wrote the paper with critical input from all of the authors.

References

1 Tripp BC, Smith K & Ferry JG (2001) Carbonic anhydrase: new insights for an ancient enzyme. *J Biol Chem* **276**, 48615–48618.
2 Zimmerman SA & Ferry JG (2008) The beta and gamma classes of carbonic anhydrase. *Curr Pharm Des* **14**, 716–721.
3 Lane TW, Saito MA, George GN, Pickering IJ, Prince RC & Morel FMM (2005) Biochemistry: a cadmium enzyme from a marine diatom. *Nature* **435**, 42.
4 Rowlett RS (2010) Structure and catalytic mechanism of the beta-carbonic anhydrases. *Biochim Biophys Acta* **1804**, 362–373.
5 Sassetti CM, Boyd DH & Rubin EJ (2003) Genes required for mycobacterial growth defined by high density mutagenesis. *Mol Microbiol* **48**, 77–84.
6 Betts JC, Lukey PT, Robb LC, McAdam RA & Duncan K (2002) Evaluation of a nutrient starvation model of *Mycobacterium tuberculosis* persistence by gene and protein expression profiling. *Mol Microbiol* **43**, 717–731.
7 Suarez Covarrubias A, Bergfors T, Jones TA & Högbom M (2006) Structural mechanics of the pH-dependent activity of beta-carbonic anhydrase from *Mycobacterium tuberculosis*. *J Biol Chem* **281**, 4993–4999.
8 Kimber MS & Pai EF (2000) The active site architecture of *Pisum sativum* beta-carbonic anhydrase is a mirror image of that of alpha-carbonic anhydrases. *EMBO J* **19**, 1407–1418.
9 von Gnielinski N, Nienaber L, Mason L, Ellis S, Triccas JA, Davis RA & Hofmann A (2014) Non-classical beta-carbonic anhydrase inhibitors – towards novel anti-mycobacterials. *MedChemComm* **5**, 1563–1566.
10 Wayne LG & Sohaskey CD (2001) Nonreplicating persistence of *Mycobacterium tuberculosis*. *Annu Rev Microbiol* **55**, 139–163.
11 Voskuil MI, Schnappinger D, Visconti KC, Harrell MI, Dolganov GM, Sherman DR & Schoolnik GK (2003) Inhibition of respiration by nitric oxide induces a *Mycobacterium tuberculosis* dormancy program. *J Exp Med* **198**, 705–713.

12 Kumar A, Deshane JS, Crossman DK, Bolisetty S, Yan B, Kramnik I, Agarwal A & Steyn AJC (2008) Heme oxygenase-1-derived carbon monoxide induces the *Mycobacterium tuberculosis* dormancy regulon. *J Biol Chem* **283**, 18032–18039.
13 Shiloh MU, Manzanillo P & Cox JS (2008) *Mycobacterium tuberculosis* senses host-derived carbon monoxide during macrophage infection. *Cell Host Microbe* **3**, 323–330.
14 Schnappinger D, Ehrt S, Voskuil MI, Liu Y, Mangan JA, Monahan IM, Dolganov G, Efron B, Butcher PD, Nathan C *et al.* (2003) Transcriptional adaptation of *Mycobacterium tuberculosis* within macrophages: insights into the phagosomal environment. *J Exp Med* **198**, 693–704.
15 Bhat SA, Singh N, Trivedi A, Kansal P, Gupta P & Kumar A (2012) The mechanism of redox sensing in *Mycobacterium tuberculosis*. *Free Radic Biol Med* **53**, 1625–1641.
16 Chim N, Johnson PM & Goulding CW (2014) Insights into redox sensing metalloproteins in *Mycobacterium tuberculosis*. *J Inorg Biochem* **133**, 118–126.
17 Abas SA, Hossain MB, van Der Helm D, Schmitz FJ, Laney M, Cabuslay R & Schatzman RC (1996) Alkaloids from the Tunicate *Polycarpa aurata* from Chuuk Atoll. *J Org Chem* **61**, 2709–2712.
18 Kang H & Fenical W (1996) Polycarpine dihydrochloride: a cytotoxic dimeric disulfide alkaloid from the Indian Ocean ascidian *Polycarpa clavata*. *Tetrahedron Lett* **37**, 2369–2372.
19 Radchenko OS, Novikov VL, Willis RH, Murphy PT & Elyakov GB (1997) Synthesis of polycarpine, a cytotoxic sulfur-containing alkaloid from the ascidian *Polycarpa aurata*, and related compounds. *Tetrahedron Lett* **38**, 3581–3584.
20 Hofmann A, Wang CK, Osman A & Camp D (2010) Merging structural biology with chemical biology: structural chemistry at Eskitis. *Struct Chem* **21**, 1117–1129.
21 Dictionary of Natural Products Database (2015) Taylor & Francis Group.
22 Suarez Covarrubias A, Larsson AM, Högbom M, Lindberg J, Bergfors T, Björkelid C, Mowbray SL, Unge T & Jones TA (2005) Structure and function of carbonic anhydrases from *Mycobacterium tuberculosis*. *J Biol Chem* **280**, 18782–18789.
23 Ehrt S & Schnappinger D (2009) Mycobacterial survival strategies in the phagosome: defence against host stresses. *Cell Microbiol* **11**, 1170–1178.
24 Thakur KG, Praveena T & Gopal B (2010) Structural and biochemical bases for the redox sensitivity of *Mycobacterium tuberculosis* RslA. *J Mol Biol* **397**, 1199–1208.
25 Schoepfer R (1993) The pRSET family of T7 promoter expression vectors for *Escherichia coli*. *Gene* **124**, 83–85.
26 Stratagene (2004) Quikchange® multi site-directed mutagenesis kit. Instruction Manual, Catalog #200514, Revision #113002e.
27 Hofmann A (2014) Methods in Structural Chemistry – A Lab Manual. Structural Chemistry Program, Eskitis Institute, Griffith University, Brisbane, Australia.
28 Wang CK, Weeratunga SK, Pacheco CM & Hofmann A (2012) DMAN: a Java tool for analysis of multi-well differential scanning fluorimetry experiments. *Bioinformatics* **28**, 439–440.
29 McPhillips TM, McPhillips SE, Chiu HJ, Cohen AE, Deacon AM, Ellis PJ, Garman E, Gonzalez A, Sauter NK, Phizackerley RP *et al.* (2002) Blu-Ice and the Distributed Control System: software for data acquisition and instrument control at macromolecular crystallography beamlines. *J Synchrotron Radiat* **9**, 401–406.
30 Kabsch W (1993) Automatic processing of rotation diffraction data from crystals of initially unknown symmetry and cell constants. *J Appl Crystallogr* **26**, 795–800.
31 Collaborative Computational Project Number 4 (1994) The CCP4 suite: programs for protein crystallography. *Acta Crystallogr D* **50**, 760–763.
32 Jones TA, Zou JY, Cowan S & Kjeldgaard M (1991) Improved methods for building protein models in electron density maps and location of errors in these models. *Acta Crystallogr A* **47**, 110–119.
33 Emsley P & Cowton K (2004) Coot: Model-Building Tools for Molecular Graphics. *Acta Crystallogr D* **60**, 2126–2132.
34 Adams PD, Afonine PV, Bunkóczi G, Chen VB, Davis IW, Echols N, Headd JJ, Hung L, Kapral GJ, Grosse-Kunstleve RW *et al.* (2010) PHENIX: a comprehensive Python-based system for macromolecular structure solution. *Acta Crystallogr D* **66**, 213–221.
35 Brünger AT, Adams PT, Clore GM, Delano WL, Gros P, Grosse-Kunstleve RW, Jiang JS, Kuszewski J, Nilges N, Pannu NS *et al.* (1998) Crystallography and NMR system (CNS): a new software system for macromolecular structure determination. *Acta Crystallogr D* **54**, 905–921.
36 Khalifah RG (1971) The carbon dioxide hydration activity of carbonic anhydrase. *J Biol Chem* **246**, 2561–2573.
37 Wang CK, Broder U, Weeratunga SK, Gasser RB, Loukas A & Hofmann A (2012) SBAL: a practical tool to generate and edit structure-based amino acid sequence alignments. *Bioinformatics* **28**, 1026–1027.
38 Bryson K, McGuffin LJ, Marsden RL, Ward JJ, Sodhi JS & Jones DT (2005) Protein structure prediction servers at University College London. *Nucleic Acids Res* **33**, W36–W38.

39 Wang CK & Hofmann A (2015) An integrated Java tool for generating amino acid sequence alignments with mapped secondary structure elements. *3Biotech* **5**, 87–92.
40 Brünger A (1992) Free R value: a novel statistical quantity for assessing the accuracy of crystal structures. *Nature* **355**, 472–475.
41 DeLano W (2002) The PyMOL Molecular Graphics System. http://www.pymol.org.
42 Dolinsky TJ, Czodrowski P, Li H, Nielsen JE, Jensen JH, Klebe G & Baker NA (2007) PDB2PQR: expanding and upgrading automated preparation of biomolecular structures for molecular simulations. *Nucleic Acids Res* **35**, W522–525.